



**HAL**  
open science

## Experimental study on water evaporation from compacted clay using environmental chamber

Wei-Kang Song, Yu-Jun Cui, Anh Minh A.M. Tang, Wen-Qi Ding, Qiong Wang

► **To cite this version:**

Wei-Kang Song, Yu-Jun Cui, Anh Minh A.M. Tang, Wen-Qi Ding, Qiong Wang. Experimental study on water evaporation from compacted clay using environmental chamber. *Canadian Geotechnical Journal*, 2016, 53 (8), pp.1293-1304. 10.1139/cgj-2015-0415 . hal-01515811

**HAL Id: hal-01515811**

**<https://enpc.hal.science/hal-01515811>**

Submitted on 3 May 2017

**HAL** is a multi-disciplinary open access archive for the deposit and dissemination of scientific research documents, whether they are published or not. The documents may come from teaching and research institutions in France or abroad, or from public or private research centers.

L'archive ouverte pluridisciplinaire **HAL**, est destinée au dépôt et à la diffusion de documents scientifiques de niveau recherche, publiés ou non, émanant des établissements d'enseignement et de recherche français ou étrangers, des laboratoires publics ou privés.

1 **Experimental study on water evaporation from compacted clay**  
2 **using environmental chamber**

3  
4 Wei-Kang SONG<sup>1,2,3</sup>, Yu-Jun CUI<sup>2,3</sup>, Anh Minh TANG<sup>3</sup>, Wen-Qi DING<sup>2</sup>, Qiong  
5 WANG<sup>4</sup>

6  
7 1 School of Civil Engineering, Zhengzhou University, Zhengzhou, China

8 2 Department of Geotechnical Engineering, School of Civil Engineering, Tongji  
9 University, Shanghai, China

10 3 Ecole des Ponts ParisTech, Laboratoire Navier, 6-8, avenue Blaise Pascal, 77455  
11 Marne-la-Vallée cedex 2, France

12 4 ARC Centre of Excellence for Geotechnical Science & Engineering, The University  
13 of Newcastle, Callaghan, 2308 NSW, Australia

14  
15 Corresponding Author:

16 Prof. Yu-Jun CUI

17 Ecole des Ponts ParisTech

18 6-8 avenue Blaise Pascal, Cité Descartes, Champs-sur-Marne

19 F-77455 MARNE LA VALLEE France

20  
21 Telephone: +33 1 64 15 35 50

22 Fax: +33 1 64 15 35 62

23 E-mail: yu-jun.cui@enpc.fr

24 **Abstract:**

25 Water evaporation induces large volume change for clayey soils, often causing  
26 problems to geotechnical and geoenvironmental constructions. To better understand  
27 this process, an evaporation test on a compacted clay was conducted in a large-scale  
28 environmental chamber under controlled atmospheric conditions. Atmospheric  
29 parameters (wind speed, air temperature and relative humidity) and the response of  
30 soil parameters (volumetric water content, temperature, soil suction as well as  
31 desiccation cracks) were monitored. The results show that the soil temperature is  
32 strongly related to the air conditions, evaporation process and desiccation cracks.  
33 Unlike for sand, the evolution of volumetric water content is governed by both the  
34 high water retention capacity of clay and the effect of cracks. A three-stage evolution  
35 can be observed for not only the actual evaporation rate but also the surface crack  
36 ratio. Thus, the surface crack ratio can be considered as one important parameter in  
37 the evaporation analysis taking into account the effect of desiccation cracks.

38 *Key words:* environmental chamber; compacted clay; air/soil parameters; evaporation;  
39 surface crack ratio

## 40 **Introduction**

41 Water evaporation from clayey soils can result in significant changes in soil suction,  
42 water content and temperature, giving rise to significant soil volume change and  
43 hence strongly influencing the performance of the involved geotechnical and  
44 geoenvironmental constructions: the long-term behavior of pavement and  
45 embankments/dams can significantly change due to the desiccation cracks and  
46 settlement induced by the decrease of water content (Cui et al. 2010; Puppala et al.  
47 2011, Tang et al. 2011a); buildings with shallow foundations and other geotechnical  
48 constructions can be seriously damaged due to the differential settlement induced by  
49 water evaporation (Silvestri et al. 1990; Cui and Zornberg 2008; Corti et al. 2009,  
50 2011; Qadad et al. 2012); the behavior of soil covers used in mine tailings or other  
51 hazardous waste landfills (Wilson 1990; Wilson et al. 1994, 1997; Yanful and Choo  
52 1997; Yang and Yanful 2002; Yanful et al. 2003; Cui and Zornberg 2008) and also the  
53 landfills for municipal solid waste disposal (Blight 2006, 2009) can be also strongly  
54 affected by water loss due to evaporation; the safety of high-level radioactive waste  
55 repository as a result of changes in soil hydro-mechanical properties induced by  
56 ventilation during the construction and operation periods is also an important issue  
57 (Bond et al. 2013; Millard et al. 2013). These problems clearly show the importance  
58 of well understanding the mechanisms of water evaporation from clayey soils.  
59 Indeed, when these mechanisms are well identified, it is possible to develop relevant  
60 water evaporation models for predicting soil deformation/settlement (e.g., Hemmati et  
61 al. 2010, 2012; Cui et al. 2013), and for designing geotechnical and geoenvironmental

62 constructions such as soil covers (e.g., Yanful and Choo 1997; Yanful et al. 2003).  
63  
64 Up to now, many experiments were conducted to investigate water evaporation from  
65 clayey soils. For instance, an evaporation experiment was performed by Garnier et al.  
66 (1997) on a swelling soil sample (48 mm in diameter and 50 mm in height) to  
67 determine the evaporation rate and soil hydraulic properties of soil. Yanful and Choo  
68 (1997) performed an evaporation test using an environmental chamber on a clay  
69 considered as a candidate cover soil. A clear evolution of drying front was observed  
70 through the water content profile; moreover, it was found that the soil temperature  
71 firstly decreases and then increases during evaporation and the evolution of  
72 evaporation rate presents typical three stages. Later, Yang and Yanful (2002) and  
73 Yanful et al. (2003) investigated the evaporation and drainage phenomena on a  
74 compacted sample of Halton clayey till (115 mm in diameter and 255 mm in height)  
75 with both constant (Yanful et al. 2003) and variable water table (Yang and Yanful  
76 2002). The results showed that water table change has no significant effect on the  
77 evaporation and drainage processes, verifying the effectiveness of this soil for an  
78 oxygen barrier in sulfide-bearing mine waste covers. Wilson et al. (1997) studied the  
79 Regina clay with a small sample of 0.2-0.3 m thick and found that the ratio of actual  
80 evaporation rate to potential evaporation rate and soil suction show a unique  
81 relationship, independent of soil properties and drying time. Lee et al. (2003)  
82 performed evaporation tests on Yulchon clay using a column of 240 mm diameter and  
83 800 mm height and the results were used to verify a model of water evaporation rate

84 from the surface of a deformable material.

85

86 On the other hand, desiccation cracking occurs easily for clayey soils upon drying.

87 Many studies were conducted to the evolution of soil cracking with changes in water

88 content. Nahlawi and Kodikara (2006) conducted a series of desiccation cracking tests

89 on a thin clayey soil layer in some narrow perspex and metal molds under controlled

90 relative humidity and temperature conditions. They observed that the water content at

91 crack initiation generally increases with the increase of clay layer thickness. The

92 water content values at the end of the tests under different initial conditions are

93 similar when the air condition is the same. Tang et al. (2010) performed desiccation

94 tests on soils from slurry state in a glass cup. They found that the initial critical water

95 content which corresponds to the initiation of desiccation cracking increases with

96 temperature. By contrast, the final critical water content which corresponds to the

97 transition point where the surface crack ratio trends to reach a stable value is not

98 significantly affected by temperature. Péron et al. (2006) carried out both free

99 desiccation tests and constrained desiccation tests on a slurry clayey soil for

100 investigating the mechanisms of desiccation cracking. They reported that the local

101 suction and water content values at cracking initiation are close to the air entry values.

102 Tang et al. (2011*b*) conducted desiccation tests on different soils for investigating the

103 wetting-drying effect. They found that the water content at cracking initiation

104 increases rapidly during the first three drying paths, and change slightly during the

105 subsequent drying paths. Li and Zhang (2011) studied the initiation and development

106 of crack geometric parameters at the compacted soil surface and excavated soil  
107 surface in the field. They reported that the evolution of desiccation cracks can be  
108 divided into three stages: initial stage, primary stage, and steady state stage. Moreover,  
109 when the water content reaches a critical value cracks develop quickly, and when the  
110 water content approaches the shrinkage limit cracking reaches a steady state. Yesiller  
111 et al. (2000) reported a significant effect of fine content. In general, high suctions,  
112 rapid increases in suctions, and high amount of cracking were observed in soils with  
113 high fine contents. Summarizing, the above-mentioned studies mainly focused on the  
114 effect of temperature, thickness, soil type and wetting-drying cycles on the  
115 development of cracks, the effect of cracks on evaporation being rarely mentioned. Ta  
116 (2009) and Cui et al. (2013) conducted evaporation tests on a large Romainville clay  
117 sample (1000 mm length, 800 mm width, and 1000 mm depth) using an  
118 environmental chamber, showing significant influence of desiccation cracks on the  
119 evolution of evaporation rate.

120

121 Further examination of the experiments reported in literature shows that few tests  
122 were conducted with full control of atmospheric conditions and complete  
123 measurement of soil response to evaporation. Indeed, in most experiments the soil  
124 was poorly instrumented (e.g., Wilson et al. 1997; Garnier et al. 1997; Yanful and  
125 Choo 1997; Yang and Yanful 2002; Yanful et al. 2003; Lee et al. 2003), although the  
126 water evaporation process has been recognized to be governed by both atmospheric  
127 and soil conditions for bare soils.

128

129 In this study, the process of water evaporation was investigated on a compacted clay  
130 sample (1000 mm×800 mm×250 mm) in a large-scale environmental chamber which  
131 was previously used for investigating water evaporation from sand (Song et al. 2013,  
132 2014) under controlled atmospheric conditions (i.e., controlled air relative humidity,  
133 temperature and air flow rate) and with a steady water table. The atmospheric  
134 parameters (air temperature, relative humidity) and the response of soil parameters  
135 (soil temperature, volumetric water content, matric suction and surface crack ratio)  
136 were monitored by various sensors for 83 days, including the soil parameters on the  
137 surface (soil surface temperature and matric suction). The obtained results help better  
138 understand the mechanisms of water evaporation from clayey soils, and they can also  
139 be used for further theoretical and numerical analyses.

140

## 141 **Materials**

142 The clayey soil selected for this investigation was used for the construction of an  
143 experimental embankment in Héricourt, France. Its geotechnical properties are  
144 presented in Table 1. The soil is a highly plastic clay according to the Casagrande's  
145 classification criterion and belongs to the CH group following the unified soil  
146 classification system (USCS). The grain size distribution curve determined by wet  
147 sieving and sedimentation is shown in Fig. 1.

148

## 149 **Experimental set-up**

150 The evaporation test was performed in a specially designed environmental chamber  
151 system (Fig. 2). The environmental chamber system is a large acrylic transparent  
152 chamber combined with wind supply unit (Fig. 3), air collection unit (Fig. 4a),  
153 photograph collection unit (Fig. 4b), water supply unit (Fig. 4c) and data logging  
154 system (Fig. 4d), controlling the changes of atmospheric conditions and monitoring  
155 the evolution of soil responses. In the evaporation test, the compressed air was firstly  
156 adjusted by the air flow regulator and the real flow was measured by a flowmeter  
157 (Fig. 3a). Then, it was heated using heating hoses (Fig. 3b) with the temperature  
158 controlled by a temperature regulator (Fig. 3c). The air temperature and relative  
159 humidity were measured before air was diffused into the chamber by an air  
160 distributor. After passing through the chamber, the air stream was gathered by the air  
161 collection unit for measuring its temperature and relative humidity (Fig. 4a). During  
162 the test, the evolution of desiccation cracks was captured by the photograph  
163 collection unit (Fig. 4b). The water table was kept constant by the water supply unit,  
164 and the change of water table was monitored using a graduated tube (Fig. 4c). All  
165 data were recorded using the data logging system (Fig. 4d).

166

167 For monitoring the atmospheric conditions and the response of soil, various sensors  
168 were buried inside the soil or installed at different positions of chamber (see Figs. 2  
169 and 5). In particular, four high-capacity tensiometers were installed at different  
170 depths along the chamber wall for measuring the soil matric suction; six soil

171 moisture sensor namely ThetaProbe (ML2x) were buried at different depths for  
172 measuring the volumetric water content; five soil temperature sensors (PT1000)  
173 were installed in the soil sample at different depths; five T3111 transmitters were  
174 installed at different locations for monitoring air temperature and relative humidity;  
175 five thermistors were fixed at different heights above the soil surface for monitoring  
176 air temperature; an infrared thermometer (Pyropen-D) was installed at the chamber  
177 cover for measuring the soil surface temperature. A digital camera (Canon EOS400D)  
178 was used for taking photos of soil surface. A flowmeter (MAS-3120) and an  
179 anemometer (Testo 435-2) were used to measure the air flow rate and the  
180 corresponding wind speed inside the chamber, respectively. More details of this  
181 environmental chamber and the sensors used can be found in Song et al. (2013).  
182 Note that this chamber paid more attention to the parameters in the near soil surface  
183 zone than the one reported by Ta (2009).

184

### 185 **Test procedure**

186 The clayey soil transported from the Hércourt site was air-dried, sieved at 2 mm and  
187 then stocked in a large sealed plastic box. Note that the gravimetric water content of  
188 the clay powder was 6.4 %. Prior to soil compaction, a 6.5 mm thick gravel layer was  
189 compacted on a geotextile layer above the bottom of chamber (Fig. 6a). The gravel  
190 layer surface was controlled by a level bar (Fig. 6a). This layer is termed as drainage  
191 layer. Another geotextile layer overlaid this layer and the edges of geotextile were  
192 taped to the chamber wall, avoiding migration of clay particles.

193

194 A mass of 59.58 kg of soil powder was poured into the chamber, smoothed using a  
195 wood plate with level bar (Fig. 6*b*) and compacted manually using a steel plate to  
196 have an uniform layer of 50 mm thick (Fig. 6*c*) with a dry density of  $1.4 \text{ Mg/m}^3$ . Note  
197 that this is also the in-situ dry density of the embankment soil at the site of Héricourt  
198 (Dong, 2013). This procedure was repeated for other layers until reaching the total  
199 height of 250 mm.

200

201 During the compaction, various sensors were installed in the soil between the layers.  
202 Five PT1000 sensors for soil temperature were installed every 50 mm (i.e., 50, 100,  
203 150, 200 and 250-mm depths) (Fig. 6*d*). All these sensors were buried in the zone  
204 300 mm far from the chamber wall (Fig. 6*d*) in order to minimize the effect of  
205 laboratory temperature changes. Six ThetaProbe sensors were buried at different  
206 depths. Three of them were at 80 mm, 130 mm and 230 mm below the soil surface,  
207 and the other three were in the near surface zone at 25, 40 and 55-mm depths,  
208 respectively. For the sake of minimizing the effect of sensor installation on the soil  
209 density, a hole with similar size as ThetaProbe was created at the defined depth for  
210 inserting the sensor (Fig. 6*e*). Then, the hole was backfilled by the same soil powder  
211 with the calculated quantity and then compacted manually to reach the same dry  
212 density of  $1.4 \text{ Mg/m}^3$ . Notably, the ThetaProbe was calibrated before installation  
213 according to the method proposed by Tang et al. (2009).

214

215 Three high-capacity tensiometers were installed at various depths (i.e., 25, 77 and  
216 173 mm below the soil surface) along two sides of chamber wall for the matrix  
217 suction measurements during the saturation process. Five thermistors measuring the  
218 air temperature were fixed at different elevations (i.e., 50, 170, 235, 330 and 425 mm  
219 above the soil surface) along one inside wall of the chamber. Two relative humidity  
220 sensors (T3111 transmitters) were installed at 50 and 275-mm heights for monitoring  
221 the air relative humidity, while three other relative humidity sensors were installed for  
222 recording the relative humidity at inlet, outlet and in the laboratory. One tensiometer  
223 was installed at a depth of 15 mm below the soil surface for measuring the near  
224 surface matric suction. An anemometer with a telescopic handle was fixed at one side  
225 of the chamber cover, allowing measuring the wind speed at 50 mm above the soil  
226 surface. After these sensors were installed, the chamber cover was sealed by silicon to  
227 ensure the air-tightness. Moreover, an infrared thermometer was fixed on the cover to  
228 monitor the soil or water surface temperature at the center. Four Light Emitting  
229 Diodes (LEDs) were installed around the four edges of the transparent chamber cover,  
230 allowing the soil surface to be lighted for better photographing.

231  
232 Finally, the bottom of chamber was connected to a water tank with its water level kept  
233 at the level of the soil surface. The saturation process was then performed with water  
234 flow from soil bottom firstly and then from soil surface for accelerating this process.  
235 Finally, a water layer was formed on the soil surface and the volumetric water content  
236 sensors showed stable values. After the saturation, the evaporation experiment was

237 started by imposing an air flow of 155 L/min and with a thin water layer (6-15 mm in  
 238 thickness) on soil surface. The inlet air was heated at a temperature as high as 200 °C,  
 239 so that a quite low relative humidity (1.5 % to 3 %) and a high temperature ( $56 \pm 4$  °C)  
 240 at the inlet of the chamber were obtained. Furthermore, photographs of soil cracks  
 241 were taken every 90 min. The surface crack ratio defined as the ratio of the surface  
 242 area of cracks to the total initial surface area can be then determined using the digital  
 243 image processing technique (see Tang et al. 2008). Note that the water level was  
 244 controlled at the initial location by regularly adding water to the tank and the quantity  
 245 of water added was also recorded.

246  
 247 The evaporation rate was determined based on the change of absolute humidity at the  
 248 inlet and outlet of chamber and the air flow rate, as follows:

$$249 \quad [1] \quad E = 86400Q(h_{outlet} - h_{inlet})/(\rho_w A)$$

250 where  $E$  is the actual evaporation rate (mm/day),  $h_{outlet}$  is the absolute humidity of air  
 251 flow at the outlet of chamber ( $\text{Mg}/\text{m}^3$ ),  $h_{inlet}$  is the absolute humidity of air flow at the  
 252 inlet of chamber ( $\text{Mg}/\text{m}^3$ ),  $Q$  is the air flow rate through the chamber (L/s),  $\rho_w$  is the  
 253 water density ( $\text{Mg}/\text{m}^3$ ), and  $A$  is the evaporative surface area of soil in the chamber  
 254 ( $\text{m}^2$ ).

255  
 256 More details about this method can be found in the works of Mohamed et al. (2000),  
 257 Aluwihare and Watanabe (2003) and Song et al. (2013, 2014).

258

## 259 **Results and discussion**

260

261 Figure 7 depicts the evolution of air flow rate versus elapsed time. The air supply unit  
262 provided compressed hot air at a rate as high as 155 L/min (average value) with a  
263 fluctuation of  $\pm 5$  L/min. The value remained at 153 L/min in the first 1.9 days, and  
264 then increased to 165 L/min and remained at this value until  $t = 30$  days. Afterwards,  
265 it decreased to 150 L/min.

266

267 The evolution of wind speed measured by anemometer at 50-mm height is presented  
268 in Fig. 8. The high air flow rate resulted in a wind speed as high as 0.4 m/s (average  
269 value) in the chamber. Note that the fluctuation of wind speed was induced by  
270 changes of air flow rate in the laboratory air compression system.

271

272 The changes of air temperature at the inlet and outlet and in the laboratory are shown  
273 in Fig. 9. On the whole, the air temperature was relatively constant. The highest air  
274 temperature was for the inlet with a value as high as  $56 \pm 4$  °C, whereas the value at  
275 the outlet was lower and was increasing during the test from 26.5 °C to 33 °C. The  
276 laboratory room temperature varied from 17 °C to 24.5 °C and was lower than those  
277 at the inlet and outlet.

278

279 Figure 10 shows changes in air temperature over time at various positions. The values  
280 varied between 22 °C and 32 °C, following the evolution of air temperature at the  
281 inlet of chamber. The lowest value was for the 50-mm height. Furthermore, the values

282 were quite similar in the zone above 50-mm height and they are therefore termed as  
283 “other heights” in this figure. Note that only the values at 50, 170, 235, and 330-mm  
284 heights were recorded.

285

286 The evolution of soil temperature is shown in Fig. 11. In general, the soil temperatures  
287 fluctuated during the whole test period except a relative stable stage occurring in the  
288 first 15 days. The highest temperature occurred at the soil surface; it remained around  
289 21 °C during the first 15 days, and then significantly increased up to 29 °C at  $t = 29$   
290 days. Afterwards, it varied between 26 °C and 31.1 °C until the end of test. For the  
291 temperatures at deeper levels (50, 100, 150, 200 and 250-mm depths), the values were  
292 very close and varied between 18 °C and 24 °C during the 83-day evaporation test  
293 except the near stabilization stage with a value around 20.5 °C in the first 15 days.  
294 This is probably due to a stable energy exchange between the energy for evaporation  
295 and for heating the soil by hot air in this stage. Note that the values at 100, 150 and  
296 200-mm depths are termed as “other depths” in this figure. Actually, all values of  
297 temperature at different depths decreased in the first day; the lowest value occurred at  
298 50-mm depth and the highest one at 250-mm depth. Afterwards, the values remained  
299 stable until  $t = 15$  days. Then, the values fluctuated over time and they decreased over  
300 depth after  $t = 19.8$  days, the highest value being at 50-mm depth while the lowest one  
301 being at 250-mm depth. Note that the evolution of soil temperature followed the air  
302 temperature changes, especially the changes of air temperature at the inlet.

303

304 All temperature data recorded are used to plot the air-soil temperature profiles (Fig.  
305 12). Generally, the air temperature was significantly higher than the soil temperature  
306 and large temperature gradient was observed at the air-soil interface. For the air  
307 temperature, the elevations above 170-mm height presented similar values and a large  
308 temperature gradient was observed from 50-mm height to the soil surface. Regarding  
309 the soil temperature changes, at the beginning of evaporation, the temperature at the  
310 soil surface was the lowest value and the temperatures below the 50-mm depth were  
311 quite similar, around 20.8 °C. Furthermore, the soil temperatures in the zone below  
312 50-mm depth showed a linear distribution over depth: the soil temperatures in this  
313 zone increased over depth before  $t = 16$  days while the trend was inversed after this  
314 time. On the other hand, a large temperature gradient occurred between the soil  
315 surface and the 50-mm depth and it became larger and larger after  $t = 16$  days.  
316 However, the temperature gradient below this depth was small. Beyond the  
317 phenomena listed above, the soil temperature also increased with the increase of air  
318 temperature, suggesting that the energy for evaporation was from the hot air and that  
319 part of the energy was used for heating soil and air. Moreover, the decrease of  
320 temperature gradient between 50-mm height and soil surface can be attributed to the  
321 increasing energy used for heating soil and air when the evaporation rate decreased.  
322 The enlarged temperature gradient between the soil surface and the 50-mm depth  
323 showed a deepening of the drying front, as observed in the sand evaporation test  
324 (Song et al. 2013, 2014). For the soil temperature evolution, the changes of soil  
325 temperature with air temperature changes were found larger in clay than in sand (see

326 Song et al. 2014). This phenomenon may be attributed to the effect of desiccation  
327 cracks: cracks change the evaporation process from one-dimensional to  
328 three-dimensional situation, allowing the air condition to affect the soil temperature in  
329 deeper zones through them.

330

331 The changes of air relative humidity are shown in Fig. 13. The imposed relative  
332 humidity at the inlet was extremely low, ranging from 1.5 % to 3 %. The values at  
333 other locations were much higher and showed a decreasing trend: the values at the  
334 outlet and at 235-mm height decreased from 40 % to 11 %; the value at 50-mm height  
335 was the highest and varied from 13 % to 55 %. On the other hand, the relative  
336 humidity in the laboratory varied with a large fluctuation between 10 % and 50 %, and  
337 presented a quite different evolution pattern with respect to other positions. On  
338 the whole, the variations of relative humidity in the chamber (50, 235-mm depth and  
339 outlet) can be divided into three parts: (1) a decrease with quite low rate in the first 15  
340 days; (2) a sharply decline until  $t = 28$  days; and (3) a slow decrease followed by a  
341 stabilization at the end of test. More precisely, the relative humidity at 50-mm height  
342 declined slowly from 55 % to 41 % during the first 15 days, then significantly from  
343 41 % to 19 % until  $t = 28$  days, and finally reached a value as low as 13 % at the end  
344 of test. Furthermore, the value at 235-mm height was a little higher than that at the  
345 outlet in the first 16 days and then they became similar during the rest of time. Note  
346 that the similar three-stage evolution of air relative humidity inside the chamber was  
347 found in the sand evaporation test (Song et al. 2014) and clay evaporation test (Ta

348 2009). This phenomenon can be attributed to the loss of water vapor from soil with  
349 the decreasing evaporation rate.

350

351 Figure 14 presents the evolutions of volumetric water content at different depths. It  
352 appears that the volumetric water content of soil depends on both time and location.

353 Indeed, all values decreased over time: the value decreased from 62 % to 11.6 % at  
354 25-mm depth, from 59 % to 11.8 % at 40-mm depth, from 57.3 % to 20 % at 55-mm

355 depth, from 57 % to 30 % at 80-mm depth, from 57.6 % to 36.8 % at 130-mm depth  
356 and from 59.2 % to 42 % at 230-mm depth. On the other hand, the deeper the location

357 the later the initiation of water content decrease: the water content started to decrease  
358 at  $t = 5$  days at 25-mm depth, at  $t = 7$  days at 80-mm depth. In the deeper locations, it

359 began to decrease at  $t = 24$  days and  $t = 50$  days at 130 and 230-mm depths,  
360 respectively. As far as the first 80-mm layer near the soil surface is concerned, a

361 three-part evolution can be identified (at 25 and 40-mm depth): at the beginning, the  
362 volumetric water content remained at the initial value, and then sharply decreased

363 from  $t = 6$  days to  $t = 50$  days. Afterwards, it decreased at a lower rate and reached the  
364 stabilization at the end of test. For the volumetric water content at other two locations,

365 the values remained stable within the first 7 days, and then presented a constant  
366 decrease trend in the rest of time. Note that the difference of volumetric water content

367 between these two locations became larger after  $t = 25$  days.

368

369 The profiles of volumetric water content are shown in Fig. 15. The evolution of water

370 loss over depth can be clearly identified in this figure, as well as the influence depth  
371 of evaporation. In the beginning of test, the volumetric water content showed a  
372 uniform distribution over depth except in the near surface zone (55-mm depth). At the  
373 beginning of evaporation, the volumetric water contents in the zone below 55-mm  
374 depth were around 57.8 % while the values above this position were a little higher due  
375 to the decrease of density during the previous saturation process. In the first 6 days,  
376 only little water loss was observed in the zone above 40-mm depth. Then, a large  
377 amount of water was lost in the zone of 130-mm depth. Furthermore, the decrease of  
378 water content in the zone of 55-mm depth became quite slow after  $t = 48$  days while  
379 that in deeper zone became faster, indicating that water evaporation was mainly from  
380 the deeper levels after this time. Finally, the values of volumetric water content at 25  
381 and 40-mm depths were around 12 % and only the water content in the zone below  
382 130-mm depth presented a clear decrease. Note that the final water contents at 25 and  
383 40-mm depths were close to the initial water content after compaction (i.e.,  
384 10-11.8 %). On the other hand, as in the evaporation tests on sand (Song et al. 2014),  
385 a linear relationship between water content and depth can be identified and this  
386 gradient developed progressively toward the deeper zones. For instance, the linear  
387 profile appeared in the first 55 mm depth zone from the beginning to  $t = 60$  days; it  
388 was observed from the 40-mm depth to the 80-mm depth after this time. This gradient  
389 was also the maximum for the whole depth.

390

391 The evolutions of volumetric water content at various depths can be clearly evidenced

392 through the contour map (Fig. 16). On the whole, the lines with low water content  
393 values appeared later than with higher ones: the line with 60 % water content  
394 appeared at the initiation of evaporation; the line with 50 % water content at  $t = 13.5$   
395 days; the line with 30 % water content at  $t = 26$  days and the line with 15 % water  
396 content at  $t = 39$  days. Furthermore, the lines advanced toward deeper zones,  
397 indicating that water loss gradually deepened. On the other hand, the  
398 densely-distributed contour lines in the zone of 80-mm depth indicated a large water  
399 loss. In other words, water evaporation occurred mainly in this zone. The evolutions  
400 of volumetric water content at each depth can also be observed in this figure. For the  
401 water content at 25-mm depth, the value decreased to 60 % at  $t = 6.4$  days; it declined  
402 to 50 % at  $t = 13$  days, to 40 % at  $t = 14.2$  days, to 30 % at  $t = 26.3$  days and to 20 %  
403 at  $t = 32.8$  days. Finally, it became lower than 15 % after  $t = 39$  days.

404  
405 Fig. 14 confirms that the dense installation of sensors in the near surface zone allows  
406 a good monitoring of volumetric water content, avoiding determining the water  
407 content by the destructive oven-drying method (e.g., Ta 2009). In general, the surface  
408 soil layer lost water firstly and the deeper zone started to lose water only by the end of  
409 test. Similar results were obtained in the sand evaporation test by Song et al. (2014).  
410 Comparison between the case of Fontainebleau sand and the case of clayey soil in this  
411 study shows that the scenarios are quite different: for the clay, only the water content  
412 at 25-mm depth decreased quickly at the initiation of evaporation, and then at deeper  
413 locations. However, for sand, the entire zone from the surface to the 55-mm depth lost  
414 water quickly. This can be attributed to the higher water retention capacity and lower

415 permeability of the clay.

416

417 Regarding the water content profiles (Fig. 15), the change of profile in the zone from  
418 the surface to the 55-mm depth at  $t = 12$  days indicated a rapid decrease of water  
419 content and suggested a possible transition of evaporation mode from  
420 one-dimensional to three-dimensional: the water inside soil evaporates only from soil  
421 surface firstly, and then from both the crack walls and soil surface. Similar  
422 phenomenon was observed by Konrad and Ayad (1997) in a field experiment. Similar  
423 evolution of water content profile was also observed in their study. A linear  
424 relationship between water content and depth was observed in the near surface zone,  
425 and this linear relationship extended to deeper zone as also observed in the sand  
426 evaporation test by Song et al. (2014). This linear relationship was also observed by  
427 Ta (2009) through measuring the water content by oven-drying.

428

429 The evolutions of soil matric suction at different depths are presented in Fig. 17. All  
430 values at various locations were increasing with water loss: the deeper the location the  
431 lower the suction and the later the initiation of increase of suction. The soil matric  
432 suction at 15-mm depth increased quickly from 10 kPa at  $t = 11$  days to 1000 kPa at  $t$   
433  $= 15.3$  days. Similarly, the suction at 25-mm depth also sharply increased up to the  
434 maximum value of 1305 kPa at  $t = 19$  days. However, the suction at 77-mm depth  
435 increased slowly from approximately 10 kPa at  $t = 13.1$  days to 30 kPa at  $t = 26$  days,  
436 and then it sharply increased up to the maximum value of 1074 kPa at  $t = 29.5$  days.

437 As far as the 173-mm depth is concerned, the value reached 10 kPa until  $t = 22.3$  days,  
438 and then it increased at a low rate up to 37 kPa at  $t = 55$  days, and finally reached its  
439 top value of 369 kPa at  $t = 63$  days. It is noted that the suction at 25-mm depth  
440 increased more quickly than that at 15-mm depth. This can be attributed to the  
441 shrinkage of soil body when undergoing evaporation. Actually, the tensiometer at  
442 25-mm depth was installed at the edge of chamber and in contact with soil, but the  
443 one at 15-mm depth was inserted into the soil from the surface. Thus, during  
444 evaporation the soil lost water and shrank. As a result, the water evaporation from the  
445 edge of soil was quicker than inside the soil.

446

447 The profiles of soil suction are shown in Fig. 18 (without considering the data at  
448 25-mm depth). It can be observed that the matric suction decreased over depth with  
449 the largest suction gradient when approaching the soil surface. The suction gradient  
450 from 15-mm to 77-mm depth increased sharply after  $t = 16$  days, from 0.06 kPa/mm  
451 at  $t = 16$  days to 20.8 kPa/mm at  $t = 19$  days. This phenomenon corresponds to a large  
452 variation of volumetric water content during these days (see Fig. 15). Furthermore, the  
453 suction gradient between 77-mm depth and 173-mm depth became larger after  $t = 19$   
454 days, indicating a deepening of evaporation process and thus an acceleration of water  
455 loss in this zone. Note that the fact that the largest suction gradient being at the  
456 surface zone was also observed in the sand evaporation experiment (Song et al. 2013,  
457 2014).

458

459 The simultaneous measurements of suction and volumetric water content at various  
460 depths allow the determination of the soil water retention curve, as shown in Fig. 19.  
461 It appears that the relationships between the water content and suction at 15-mm and  
462 25-mm depths are quite different with those at other depths. This is probably due to  
463 the difference in soil density over depth which was strongly affected by the swelling  
464 during saturation process on one hand and the development of surface desiccation  
465 cracks on the other hand. Indeed, the surface desiccation cracks increased quickly  
466 when the suction was larger than 10 kPa which corresponds to a volumetric water  
467 content of 53%.

468  
469 The actual evaporation rate determined following eq. (1) is plotted in Fig. 20. Three  
470 stages can be identified: a stage of constant value around 2.3 mm/day during the first  
471 15 days (constant-rate stage); a stage of sharp decrease down to 0.5 mm/day at  $t = 45$   
472 days (falling-rate stage); and a stage of decrease at a quite low rate of 0.3 mm/day  
473 followed by stabilization (slow-rate stage). Note that the similar three-stage evolution  
474 of actual evaporation rate was observed in the evaporation test on clayey soil  
475 conducted by Yanful and Choo (1997).

476  
477 Figure 21 presents the evolution of the surface crack ratio during evaporation. It is  
478 observed that the evolution of the surface crack ratio can also be divided into three  
479 stages as for the actual evaporation rate (Fig. 20) and the relative humidity inside the  
480 chamber (Fig.13): (1) an increase stage until  $t = 10$  days with low values close to zero;

481 (2) an rapid increase stage from  $t = 10$  days to  $t = 25.5$  days and (3) a steady stage  
482 with a value around 25.3% until the end of test. Comparing the evolutions of actual  
483 evaporation rate and surface crack ratio, a clear phenomenon can be identified: with  
484 the development of cracks, more water can be evaporated, leading to or keeping in a  
485 high evaporation rate (the constant-rate stage). With further development of cracks,  
486 there is less water being evaporated, leading to a decrease of evaporation rate (the  
487 falling-rate stage). Finally, the evaporation rate reaches the slow-rate stage and the  
488 evolution of cracks approaches a steady state when the soil water content is extremely  
489 low. This is consistent with the observation of Li and Zhang (2011). Furthermore, it is  
490 worth noting that the characteristic days for surface crack ratio do not correspond to  
491 those for the actual evaporation rate, the evolution of actual evaporation curve lags  
492 behind that of the surface crack ratio curve, suggesting that cracks are not the only  
493 factors affecting the evaporation process. It is important to mention that the surface  
494 crack ratio is an important parameter in the evaporation analysis taking into account  
495 the effect of cracks (Cui et al. 2013). In Fig. 21, the corresponding photographs of  
496 surface cracks at different times during evaporation are also shown in this figure for  
497 better appreciating the evolution of surface crack ratio.

498

499 Direct measurements of the depths and widths of cracks were carried out using a ruler,  
500 and the results are presented in Fig. 22. It is observed that the largest crack of 32 mm  
501 was in the central part of the soil surface, and the deepest crack of 230 mm was at the  
502 edges. Moreover, at the edges, cracks presented limited width variations (15-20 mm)

503 but significant depth variations (170-230 mm). This represents the influence of the  
504 chamber wall. There is no clear relationship between depth and width, their ratio  
505 varying from 1.2 to 14.

506

## 507 **Conclusions**

508 A comprehensive laboratory experiment on water evaporation from a clayey soil was  
509 investigated using a large scale environmental chamber, with controlled atmospheric  
510 conditions and constant water table. The atmospheric parameters (wind speed, air  
511 temperature, and relative humidity) and the response of soil parameters (soil  
512 temperature, volumetric water content, matric suction and surface crack ratio) were  
513 monitored. The following conclusions can be drawn:

514

515 The soil temperature is strongly affected by the air conditions, evaporation process  
516 and desiccation cracks. The soil temperature varied with the variation of air  
517 temperature. With the decrease of evaporation rate, more energy was available for  
518 heating soil. The development of cracks increased the evaporating surface and  
519 therefore enhanced the influence of air condition on the soil temperature.

520

521 An obvious temperature decrease was observed at three locations: 50-mm height, soil  
522 surface and 50-mm depth. The soil temperature increased with the increase of air  
523 temperature, suggesting that the energy for evaporation was from the hot air, and that  
524 part of the energy was used for heating soil and air. The decrease of temperature

525 gradient between the 50-mm height and the soil surface is attributed to the increasing  
526 energy used for heating soil and air along with the decreasing evaporation rate. The  
527 enlarged temperature gradient between the soil surface and the 50-mm depth suggests  
528 a deepening of the drying front.

529

530 The air relative humidity decreased with the decreasing evaporation rate. Three stages  
531 were identified: (1) a decrease at a quite low rate; (2) a sharp decline stage; (3) a slow  
532 decrease followed by stabilization.

533

534 The dense installation of sensors in the near surface zone allowed a rich  
535 measurements of volumetric water content, avoiding determining the water content by  
536 the destructive oven-drying method. The surface soil layer lost water firstly and the  
537 deeper zone started to lose water by the end of test. The evolution of volumetric water  
538 content in the near surface zone was quite different from that for sand, to be attributed  
539 to the higher water retention capacity and lower permeability of this clayey soil.

540

541 The rapid change of volumetric content profile during the early stage of evaporation  
542 in the zone from the soil surface to 55-mm depth suggested a rapid decrease of water  
543 content and a transition of evaporation mode from one-dimensional to  
544 three-dimensional. The linear relationship between water content and depth was  
545 identified for the near surface zone, as opposed to the case of sand where the linear  
546 relationship was observed for much deeper zone. Furthermore, the large change of

547 water content in the near surface zone suggests that evaporation mainly affected this  
548 zone. Obviously, the development of cracks helped to the evaporation to be extended  
549 to deeper zone.

550

551 The soil matric suction was found to decrease over depth, and the suction gradient  
552 increased over time especially in the surface zone. The evolution of suction gradient is  
553 consistent with the volumetric water content changes.

554

555 The evolution of the surface crack ratio can be divided into three stages as for the  
556 actual evaporation rate: (1) a slow increase stage with values close to zero; (2) a rapid  
557 increase stage and (3) a steady stage. The evolution of actual evaporation curve lags  
558 behind that of the surface crack ratio curve, indicating that cracks are not the only  
559 factors affecting the evaporation process.

560

561

## 562 **Acknowledgments**

563 The authors wish to acknowledge the support of the National Natural Science of  
564 China (Grant No. 51509017).

565

## 566 **References**

567 Aluwihare, S., and Watanabe, K. 2003. Measurement of evaporation on bare soil and  
568 estimating surface resistance. *Journal of Environmental Engineering*, **129**(12):  
569 1157-1168. doi: 10.1061/(ASCE)0733-9372(2003)129:12(1157).

- 570 Blight, G.E. 2006. Graded landfill requirements in South Africa-the climatic water  
571 balance classification. *Waste Management & Research*, **24**(5): 482-490. doi:  
572 10.1177/0734242X06068516.
- 573 Blight, G. 2009. Solar heating of the soil and evaporation from a soil surface.  
574 *Géotechnique*, **59**(4): 355-363. doi: 10.1680/geot.2009.59.4.355.
- 575 Bond, A., Millard, A., Nakama, S., Zhang, C., and Garritte, B. 2013. Approaches for  
576 representing hydro-mechanical coupling between sub-surface excavations and  
577 argillaceous porous media at the ventilation experiment, Mont Terri. *Journal of*  
578 *Rock Mechanics and Geotechnical Engineering*, **5**(2): 85-96. doi:  
579 10.1016/j.jrmge.2013.02.002.
- 580 Corti, T., Muccione, V., Köllner-Heck, P., Bresch, D., and Seneviratne, S.I. 2009.  
581 Simulating past droughts and associated building damages in France. *Hydrology*  
582 *and Earth System Sciences*, **13**(9): 1739-1747. doi: 10.5194/hess-13-1739-2009.
- 583 Corti, T., Wüest, M., Bresch, D., and Seneviratne S.I. 2011. Drought-induced building  
584 damages from simulations at regional scale. *Natural Hazards and Earth System*  
585 *Sciences*, **11**(12): 3335-3342. doi: 10.5194/nhess-11-3335-2011.
- 586 Cui, Y.J., and Zornberg, J.G. 2008. Water balance and evapotranspiration monitoring  
587 in geotechnical and geoenvironmental engineering. *Geotechnical and Geological*  
588 *Engineering*, **26**(6): 783-798. doi: 10.1007/s10706-008-9198-z.
- 589 Cui, Y.J., Gao, Y.B., and Ferber, V. 2010. Simulating the water content and  
590 temperature changes in an experimental embankment using meteorological data.  
591 *Engineering Geology*, **114**: 456-471. doi: 10.1016/j.enggeo.2010.06.006.

- 592 Cui, Y.J., Ta, A.N., Hemmati, S., Tang, A.M., and Gatmiri, B. 2013. Experimental and  
593 numerical investigation of soil-atmosphere interaction. *Engineering Geology*, **165**:  
594 20-28. doi:10.1016/j.enggeo.2012.03.018.
- 595 Dong, J.C. 2013. Investigation of aggregates size effect on the stiffness of lime and/or  
596 cement treated soil: from laboratory to field conditions. PhD. thesis, Université  
597 Paris-Est, Paris.
- 598 Garnier, P., Rieu, M., Boivin, P., Vauclin, M., and Baveye, P. 1997. Determining the  
599 hydraulic properties of a swelling soil from a transient evaporation experiment. *Soil  
600 Science Society of America Journal*, **61**(6): 1555-1563. doi:  
601 10.2136/sssaj1997.03615995006100060003x.
- 602 Hemmati, S., Gatmiri, B., Cui, Y.J., and Vincent, M. 2010.  
603 Soil-vegetation-atmosphere interaction by a multiphysics approach. *Journal of  
604 Multiscale Modelling*, **2**(3-4): 163-184. doi: 10.1142/S1756973710000382.
- 605 Hemmati, S., Gatmiri, B., Cui, Y.J., and Vincent, M. 2012. Thermo-hydro-mechanical  
606 modelling of soil settlements induced by soil-vegetation-atmosphere interactions.  
607 *Engineering Geology*, **139-140**: 1-16. doi: 10.1016/j.enggeo.2012.04.003.
- 608 Konrad, J.M., and Ayad, R. 1997. Desiccation of a sensitive clay: field experimental  
609 observations. *Canadian Geotechnical Journal* **34**(6): 929-942. doi:  
610 10.1139/t97-063.
- 611 Lee, I., Lee, H., Cheon, J., and Reddi L.N. 2003. Evaporation theory for deformable  
612 soils. *Journal of Geotechnical and Geoenvironmental Engineering*, **129**(11):  
613 1020-1027. doi: 10.1061/(ASCE)1090-0241(2003)129:11(1020).

- 614 Li, J.H., and Zhang, L.M. 2011. Study of desiccation crack initiation and development  
615 at ground surface. *Engineering Geology*, **123**(4): 347-358.  
616 doi:10.1016/j.enggeo.2011.09.015.
- 617 Millard, A., Bond, A., Nakama, S., Zhang, C., Barnichon, J.-D., and Garritte, B. 2013.  
618 Accounting for anisotropic effects in the prediction of the hydro-mechanical  
619 response of a ventilated tunnel in an argillaceous rock. *Journal of Rock Mechanics  
620 and Geotechnical Engineering*, **5**(2): 97-109. doi: 10.1016/j.jrmge.2012.11.001.
- 621 Mohamed, A.A., Sasaki, T., and Watanabe, K. 2000. Solute transport through  
622 unsaturated soil due to evaporation. *Journal of Environmental Engineering*, **126**(9):  
623 842-848. doi: 10.1061/(ASCE)0733-9372(2000)126:9(842).
- 624 Nahlawi, H., and Kodikara, J.K. 2006. Laboratory experiments on desiccation  
625 cracking of thin soil layers. *Geotechnical and Geological Engineering*, **24**(6):  
626 1641-1664. doi: 10.1007/s10706-005-4894-4.
- 627 Péron, H., Laloui, L., Hueckel, T., and Hu, L. 2006. Experimental study of desiccation  
628 of soil. In *Proceedings of the Fourth International Conference on Unsaturated Soils*,  
629 Carefree, Ariz, 2–6 April 2006. Geotechnical Special Publication No. 147. Edited  
630 by G.A. Miller, C.E. Zapata, S.L. Houston, and D.G. Fredlund. American Society of  
631 Civil Engineers, Reston, Va. pp. 1073–1084.
- 632 Puppala, A.J., Manosuthkij, T., Nazarian, S. and Hoyos, L.R. 2011. Threshold  
633 moisture content and matric suction potentials in expansive clays prior to initiation  
634 of cracking in pavements. *Canadian Geotechnical Journal*, **48**(4): 519-531. doi:  
635 10.1139/T10-087.

- 636 Qadad, A.A., Shahrour, I., and Rouainia, M. 2012. Influence of the soil-atmosphere  
637 exchange on the hydric profile induced in soil-structure system. *Natural Hazards  
638 and Earth System Sciences*, **12**: 2039-2049. doi:10.5194/nhess-12-2039-2012.
- 639 Silvestri, V., Soulié, M., Lafleur, J., Sarkis, G., and Bekkouche, N. 1990. Foundation  
640 problems in Champlain clays during droughts. I : Rainfall deficits in Montréal  
641 (1930-1988). *Canadian Geotechnical Journal*, **27**(3): 285-293. doi:  
642 10.1139/t90-039.
- 643 Song, W.K., Cui, Y.J., Tang, A.M., and Ding, W.Q. 2013. Development of a  
644 large-scale environmental chamber for investigating soil water evaporation.  
645 *Geotechnical Testing Journal*, **36**(6): 847-857. doi: 10.1520/GTJ20120142.
- 646 Song, W.K., Cui, Y.J., Tang, A.M., Ding, W.Q., and Tran, T.D. 2014. Experimental  
647 study on water evaporation from sand using environmental chamber. *Canadian  
648 Geotechnical Journal*, **51**(2): 115-128. doi: 10.1139/cgj-2013-0155.
- 649 Ta, A.N. 2009. Etude de l'interaction sol-atmosphère en chambre environnementale.  
650 PhD. Thesis, Ecole des Ponts Paristech, Paris.
- 651 Tang, C., Shi, B., Liu, C., Zhao, L., and Wang, B. 2008. Influencing factors of  
652 geometrical structure of surface shrinkage cracks in clayey soils. *Engineering  
653 Geology*, **101**(3-4): 204-217. doi: 10.1016/j.enggeo.2008.05.005.
- 654 Tang, A.M., Ta, A.N., Cui, Y.J., and Thiriat, J. 2009. Development of a large-scale  
655 infiltration tank for determination of the hydraulic properties of expansive clays.  
656 *Geotechnical Testing Journal*, **32**(5): 385-396. doi: 10.1520/GTJ102187.
- 657 Tang, C., Cui, Y.J., Tang, A.M., and Shi, B. 2010. Experiment evidence on the

- 658 temperature dependence of desiccation cracking behavior of clayey soils.  
659 Engineering Geology, **114**(3-4): 261-266. doi: 10.1016/j.enggeo.2010.05.003.
- 660 Tang, C., Shi, B., Liu, C., Gao, L. and Inyang, H.I. 2011a. Experimental investigation  
661 of the desiccation cracking behavior of soil layers during drying. Journal of  
662 Materials in Civil Engineering, **23**(6): 873-878. doi:  
663 10.1061/(ASCE)MT.1943-5533.0000242.
- 664 Tang, C.S., Cui, Y.J., Shi, B., Tang, A.M., and Liu, C. 2011b. Desiccation and  
665 cracking behaviour of clay layer from slurry state under wetting-drying cycles.  
666 Geoderma, **166**(1): 111-118. doi: 10.1016/j.geoderma.2011.07.018.
- 667 Wilson, G.W. 1990. Soil evaporative fluxes for geotechnical engineering problems.  
668 PhD. thesis, Department of Civil Engineering, University of Saskatchewan,  
669 Saskatoon, Sask.
- 670 Wilson, G.W., Fredlund, D.G., and Barbour, S.L. 1994. Coupled soil-atmosphere  
671 modelling for soil evaporation. Canadian Geotechnical Journal, **31**(2): 151-161.  
672 doi: 10.1139/t94-021.
- 673 Wilson, G.W., Fredlund, D.G., and Barbour, S.L. 1997. The effect of soil suction on  
674 evaporative fluxes from soil surfaces. Canadian Geotechnical Journal, **34**(1):  
675 145-155. doi: 10.1139/t96-078.
- 676 Yanful, E.K., and Choo, L.P. 1997. Measurement of evaporative fluxes from candidate  
677 cover soils. Canadian Geotechnical Journal, **34**(3): 447-459. doi: 10.1139/t97-002.
- 678 Yanful, E.K., Mousavi, S.M., and Yang, M. 2003. Modeling and measurement of  
679 evaporation in moisture-retaining soil covers. Advances in Environmental

- 680 Research, **7**(4): 783-801. doi: 10.1016/S1093-0191(02)00053-9.
- 681 Yang, M., and Yanful, E.K. 2002. Water balance during evaporation and drainage in  
682 cover soils under different water table conditions. *Advances in Environmental*  
683 *Research*, **6**(4): 505-521. doi: 10.1016/S1093-0191(01)00077-6.
- 684 Yesiller, N., Miller, C.J., Inci, G., and Yaldo, K. 2000. Desiccation and cracking  
685 behavior of three compacted landfill liner soils. *Engineering Geology*, **57**(1-2):  
686 105-121. doi: 10.1016/S0013-7952(00)00022-3.
- 687

688 **List of Tables**

689 Table 1. Geotechnical properties of the soil studied

690

691 **List of Figures**

692 Fig. 1. Grain size distribution of Héricourt clay

693 Fig. 2. Sketch of the environmental chamber system

694 Fig. 3. Wind supply unit: (a) high-pressure compressed air source and air flow rate

695 measurement unit, (b) heating hoses, (c) temperature regulator, and (d) relative

696 humidity and temperature measurement unit.

697 Fig. 4. Details of environmental chamber system (without wind supply unit): (a) air

698 collection unit, (b) photograph collection unit, (c) water supply unit, and (d)

699 data logging system.

700 Fig. 5. Distribution of sensors

701 Fig. 6. Experimental procedure: (a) laying gravel layer, (b) smoothing soil surface by

702 ruler, (c) soil compaction, (d) PT1000 installation, (e) ThetaProbe installation,

703 and (f) evaporation test initiation.

704 Fig. 7. Evolution of air flow rate

705 Fig. 8. Evolution of wind speed

706 Fig. 9. Evolutions of air temperature at the inlet and outlet of chamber as well as in

707 the laboratory

708 Fig. 10. Evolutions of air temperature at different elevations

709 Fig. 11. Evolutions of soil temperature at different positions

710 Fig. 12. Profiles of air-soil temperature

711 Fig. 13. Evolutions of air relative humidity at different positions in the chamber and

712 laboratory

713 Fig. 14. Evolutions of volumetric water content at different depths

- 714 Fig. 15. Profiles of volumetric water content
- 715 Fig. 16. Contour map of volumetric water content at different times
- 716 Fig. 17. Evolutions of matric suction at different depths
- 717 Fig. 18. Profiles of matric suction at different times
- 718 Fig. 19. Soil water retention curve obtained from the evaporation test
- 719 Fig. 20. Evolutions of actual evaporation rate
- 720 Fig. 21. Evolution of surface crack ratio
- 721 Fig. 22. Depth versus width of cracks
- 722

**Table 1.** Geotechnical properties of the soil studied

Physical property	Value
Specific gravity	2.70
Plastic limit (%)	37
Liquid limit (%)	76
Plasticity index	39
Clay (<2 $\mu$ m) content (%)	78
Blue methylene value	7.5

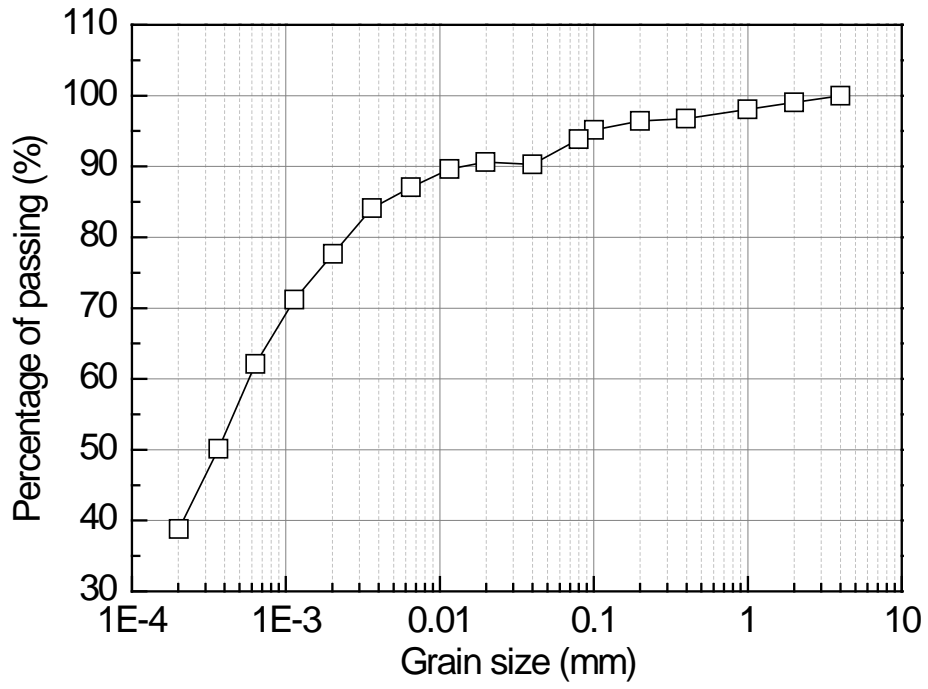


**Fig. 1.** Grain size distribution of Héricourt clay

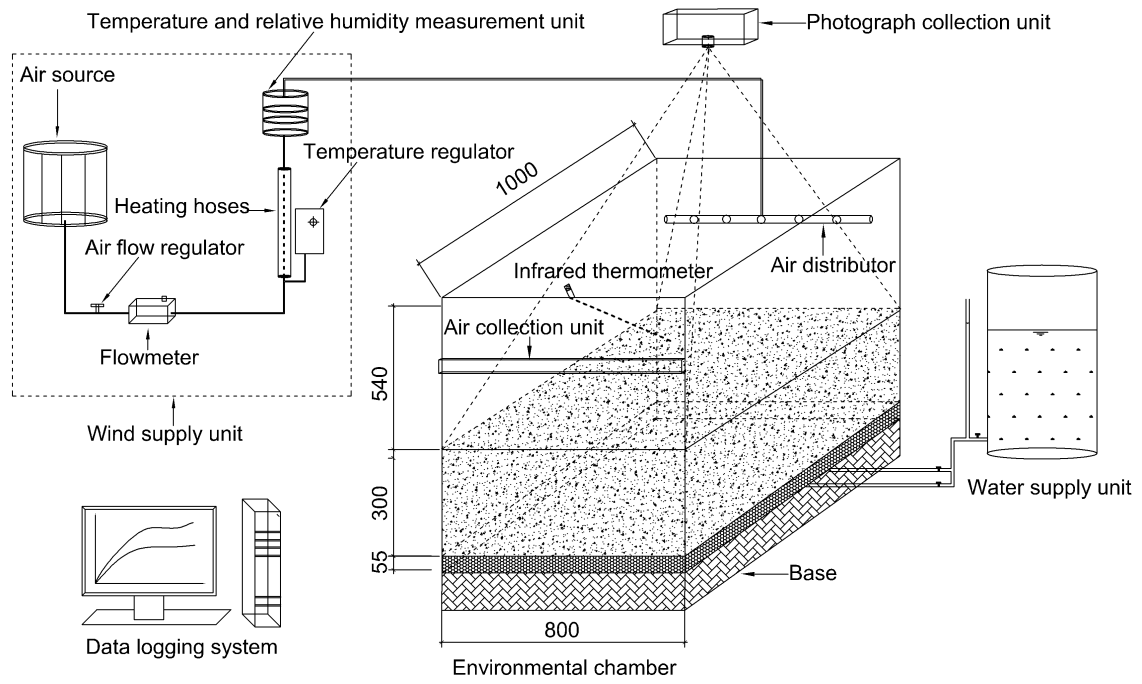


**Fig. 2.** Sketch of the environmental chamber system

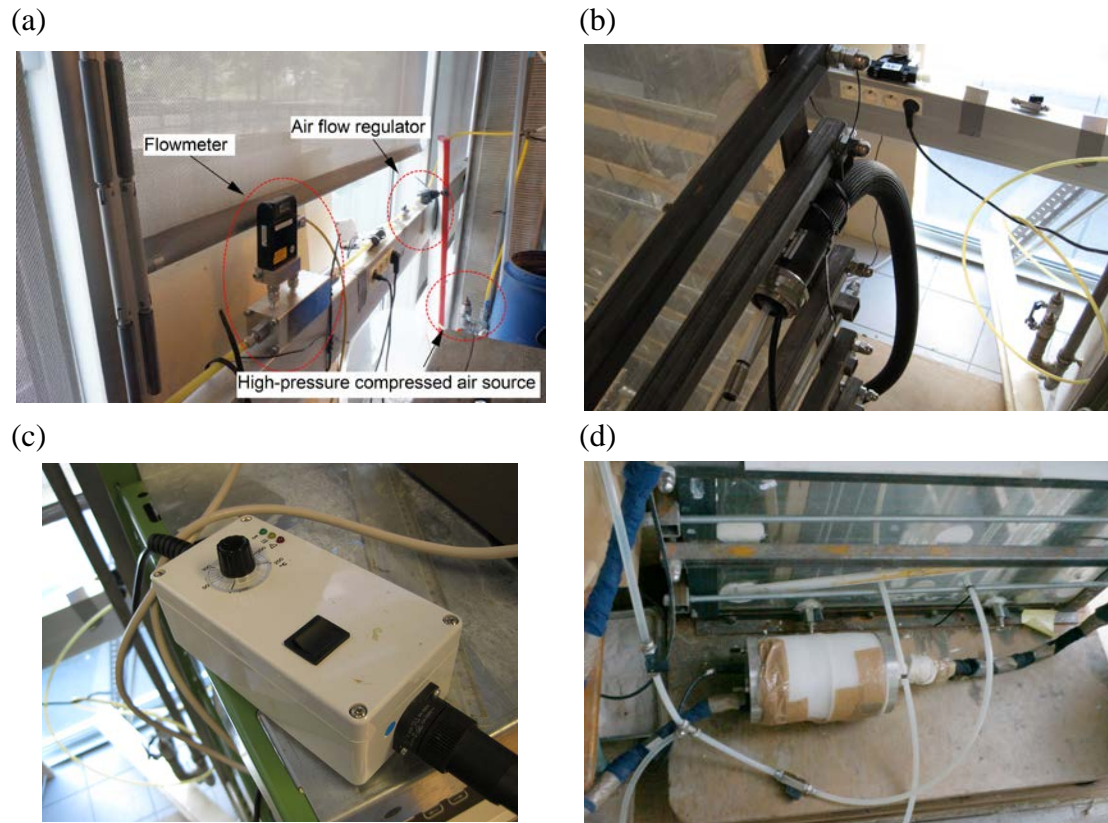


**Fig. 3.** Wind supply unit: (a) high-pressure compressed air source and air flow rate measurement unit, (b) heating hoses, (c) temperature regulator, and (d) relative humidity and temperature measurement unit.

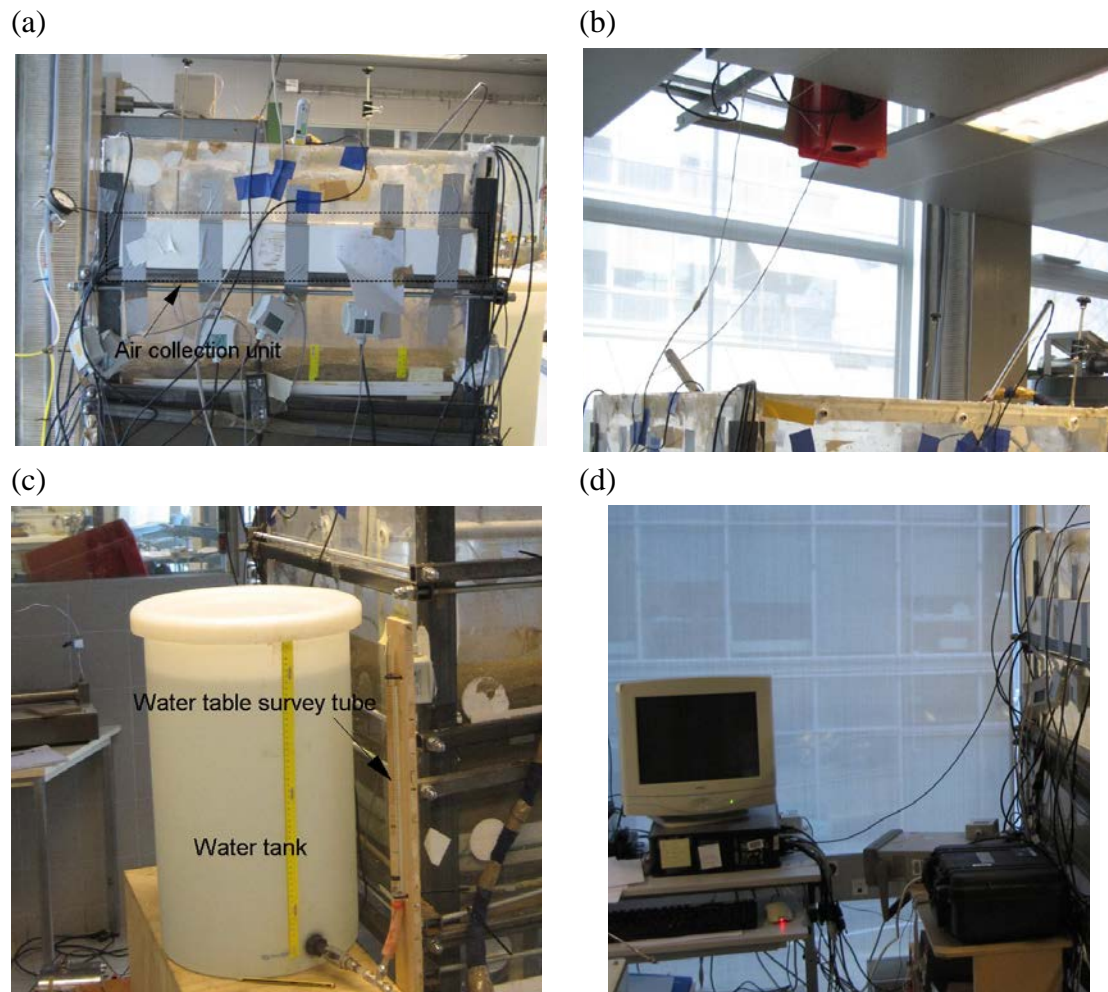


**Fig. 4.** Details of environmental chamber system (without wind supply unit): (a) air collection unit, (b) photograph collection unit, (c) water supply unit, and (d) data logging system.

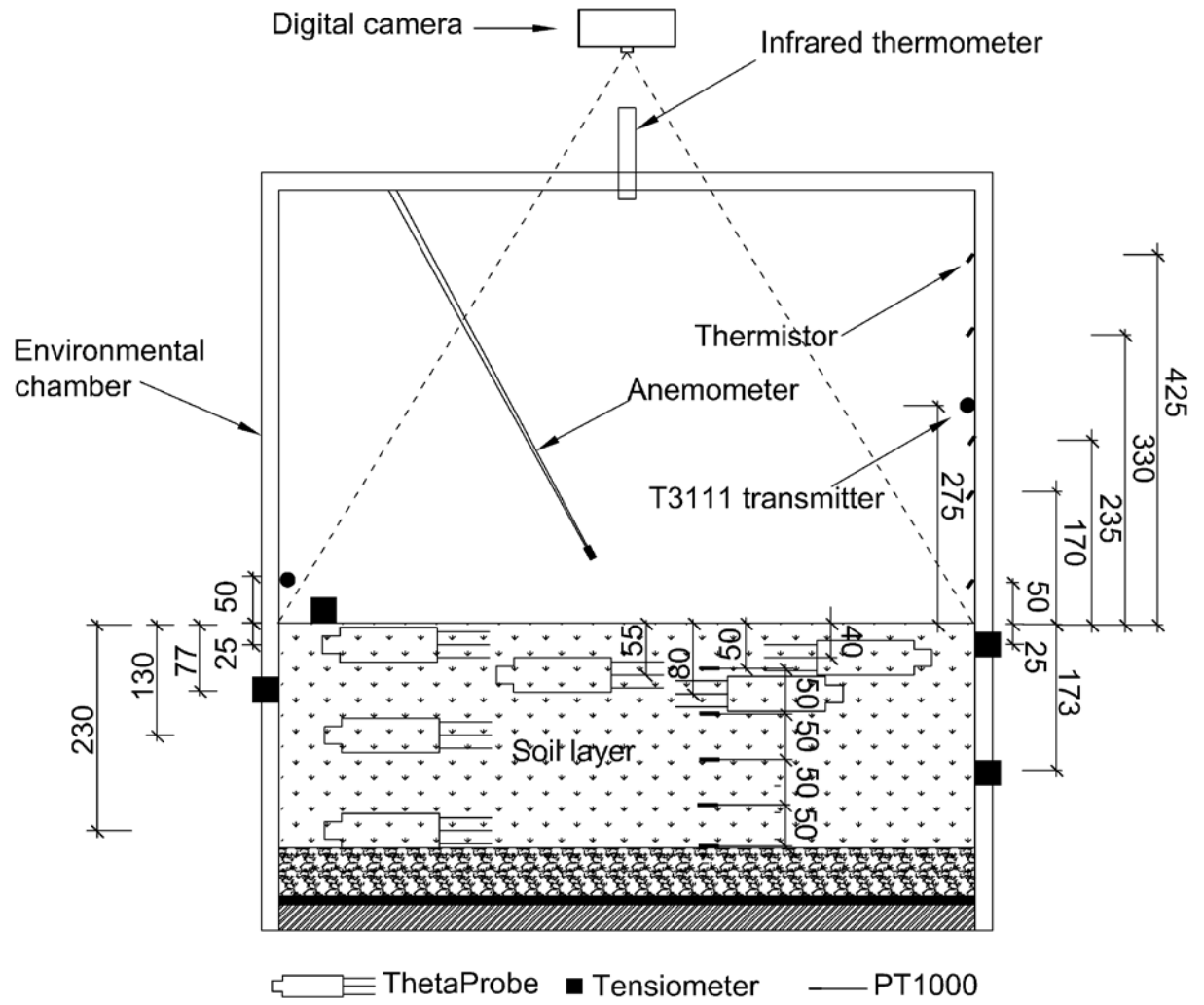


**Fig. 5.** Distribution of sensors

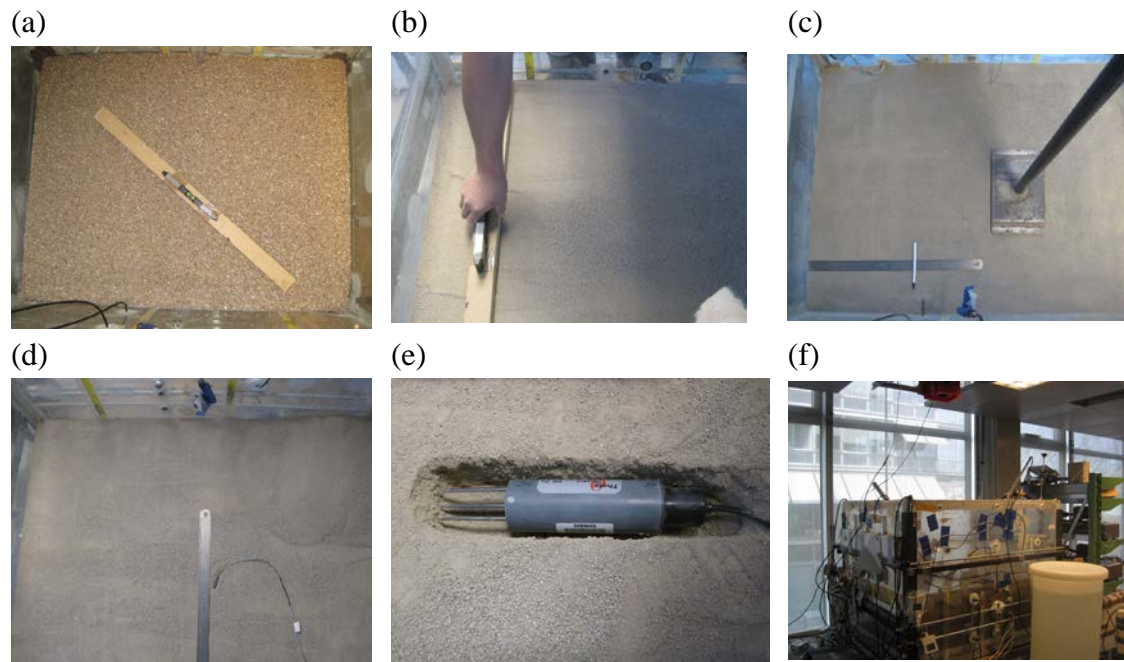


**Fig. 6.** Experimental procedure: (a) laying gravel layer, (b) smoothing soil surface by ruler, (c) soil compaction, (d) PT1000 installation, (e) ThetaProbe installation, and (f) evaporation test initiation.

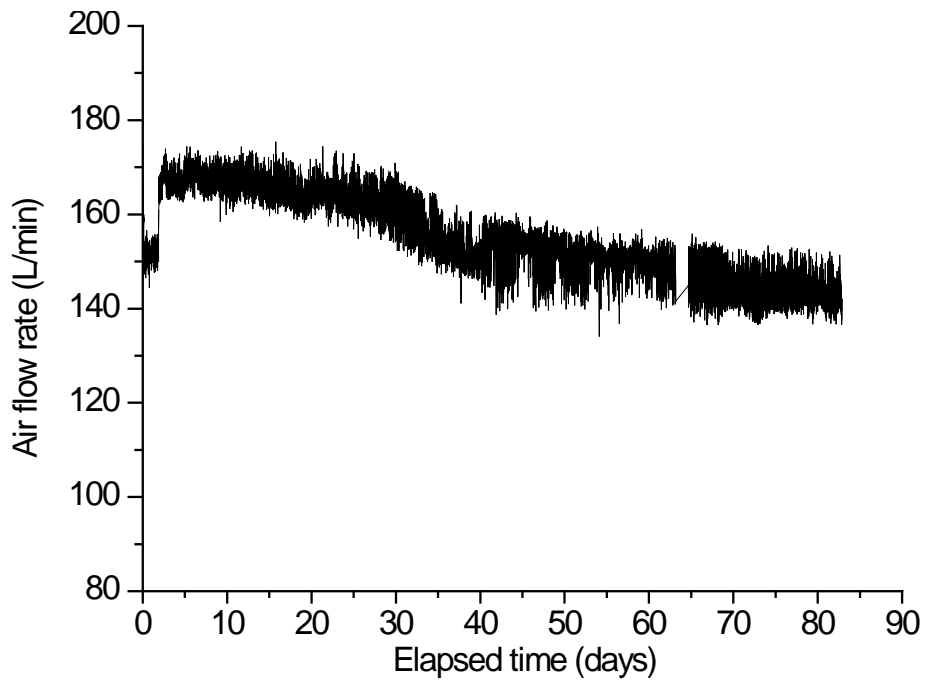


**Fig. 7.** Evolution of air flow rate

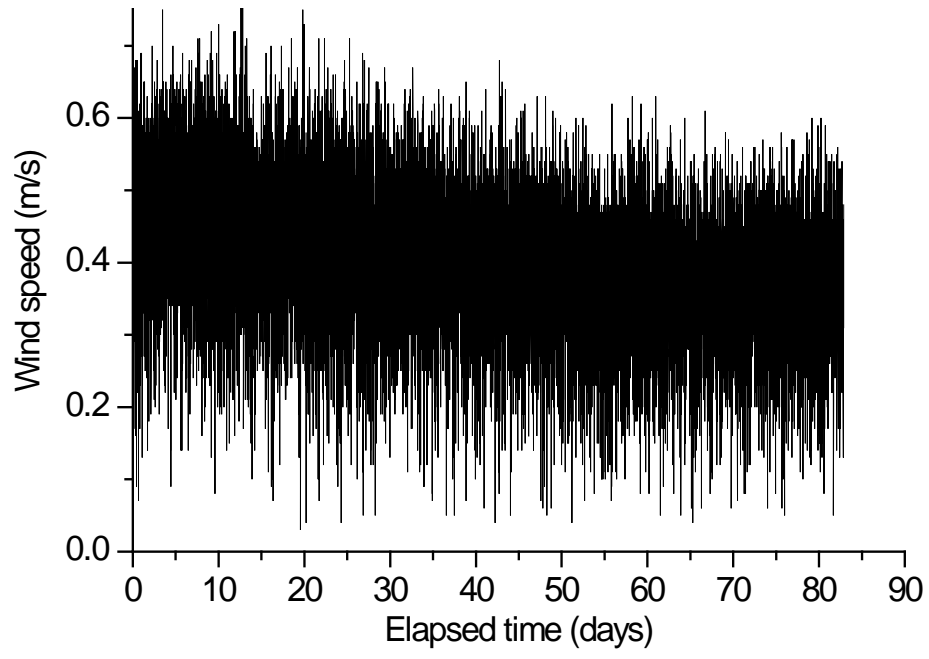


**Fig. 8.** Evolution of wind speed

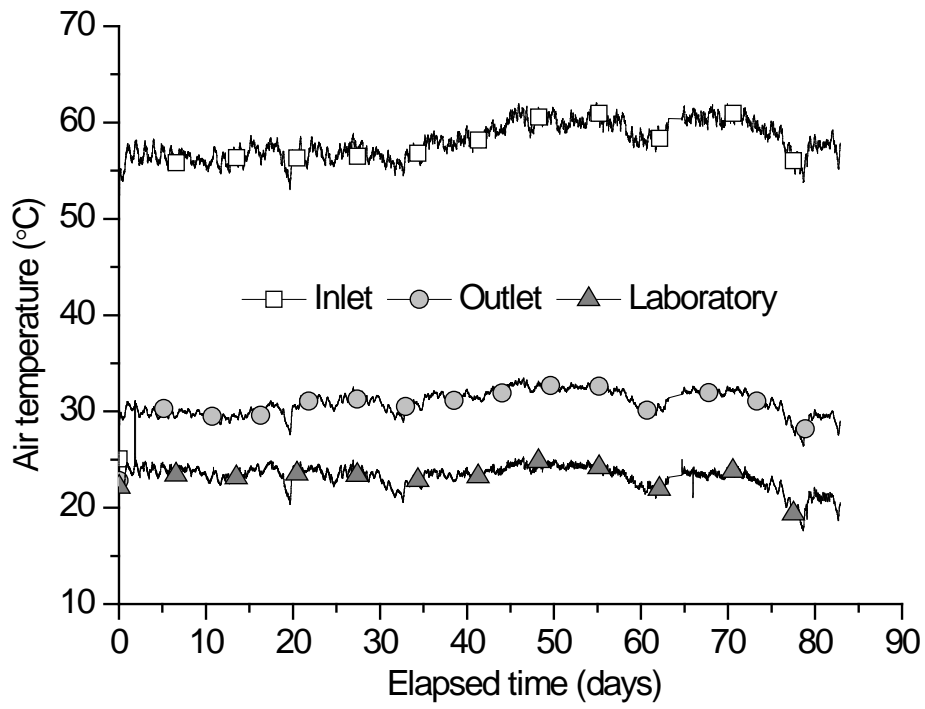


**Fig. 9.** Evolutions of air temperature at the inlet and outlet of chamber as well as in the laboratory

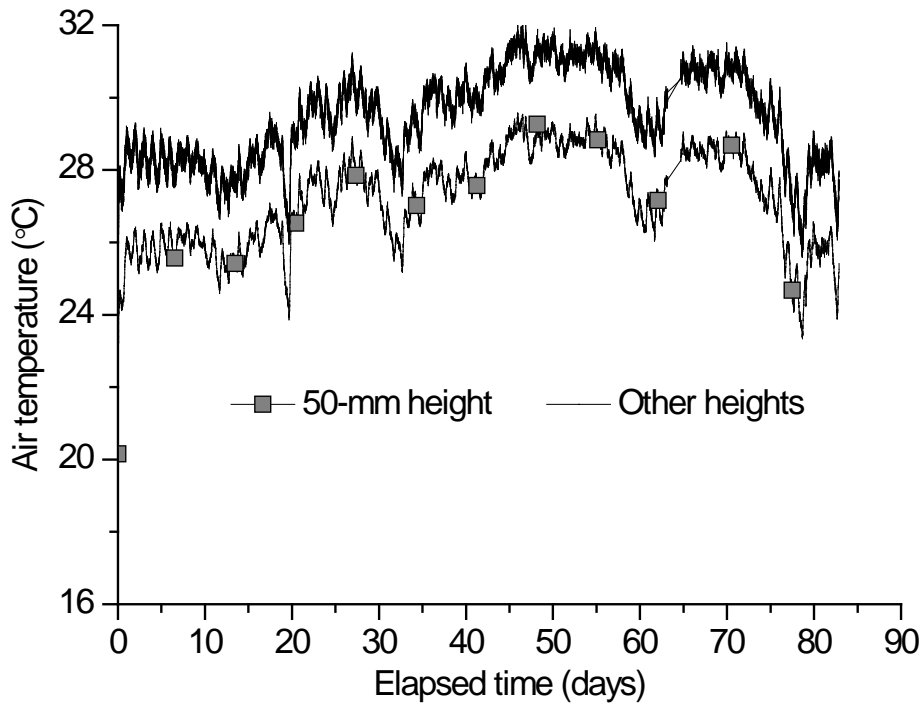


**Fig. 10.** Evolutions of air temperature at different elevations

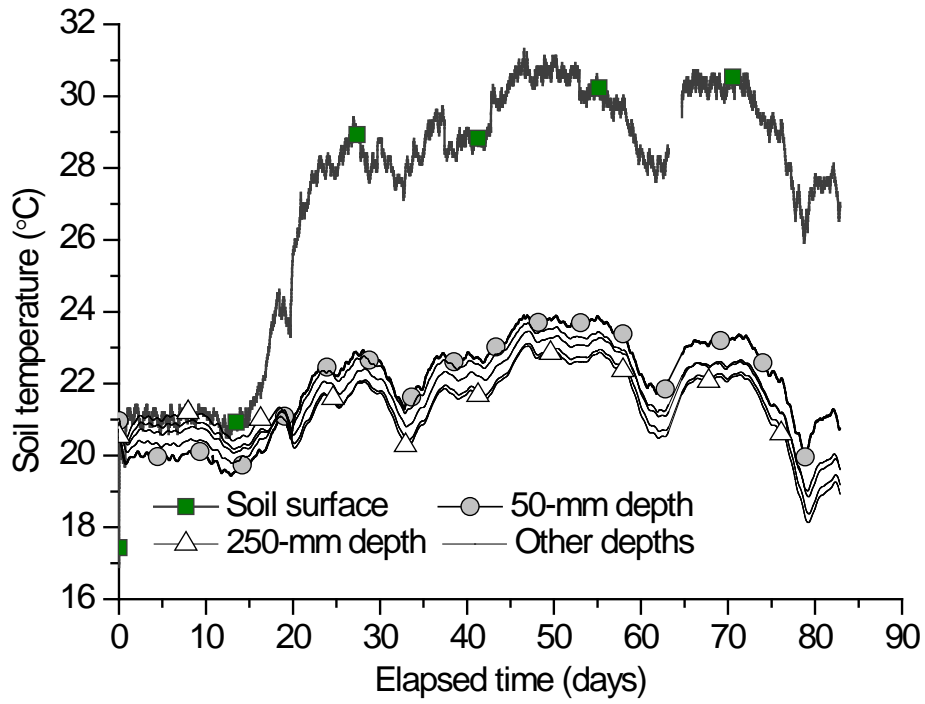


**Fig. 11.** Evolutions of soil temperature at different locations

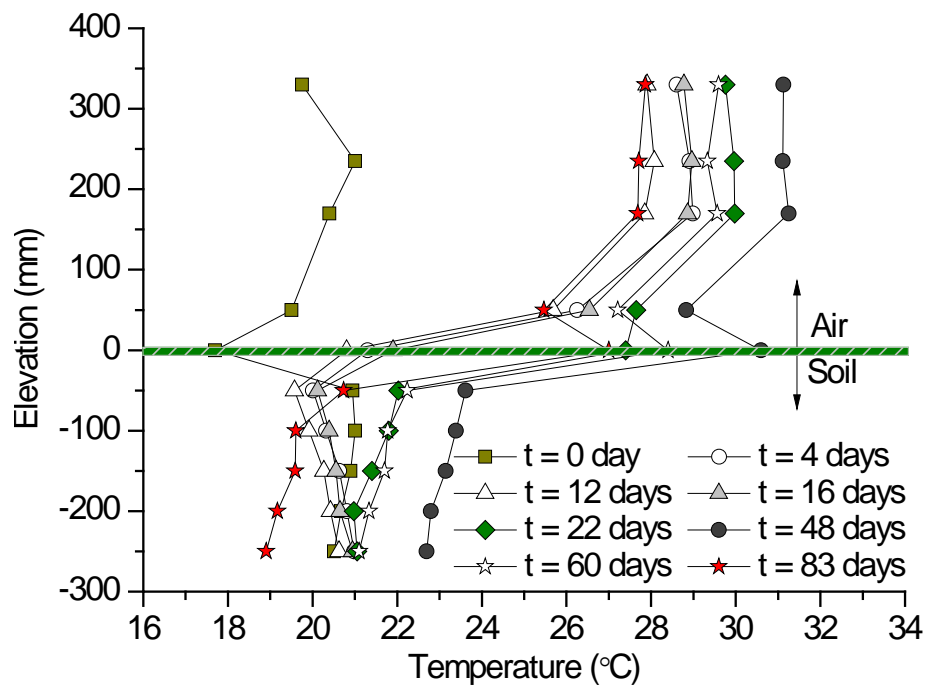


**Fig. 12.** Profiles of air-soil temperature

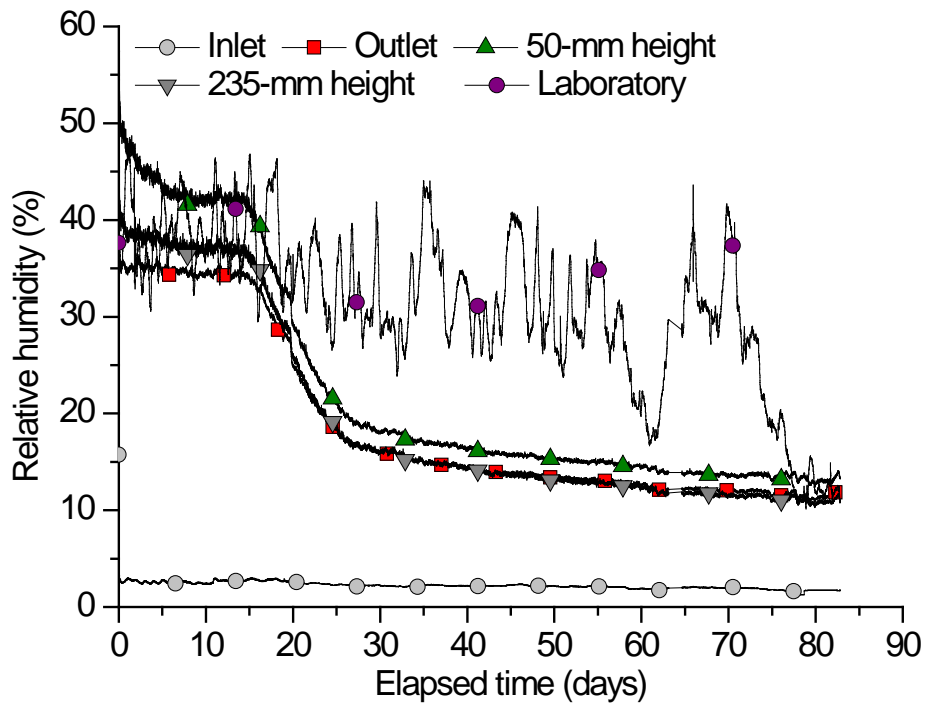


**Fig. 13.** Evolutions of air relative humidity at different locations in the chamber and laboratory

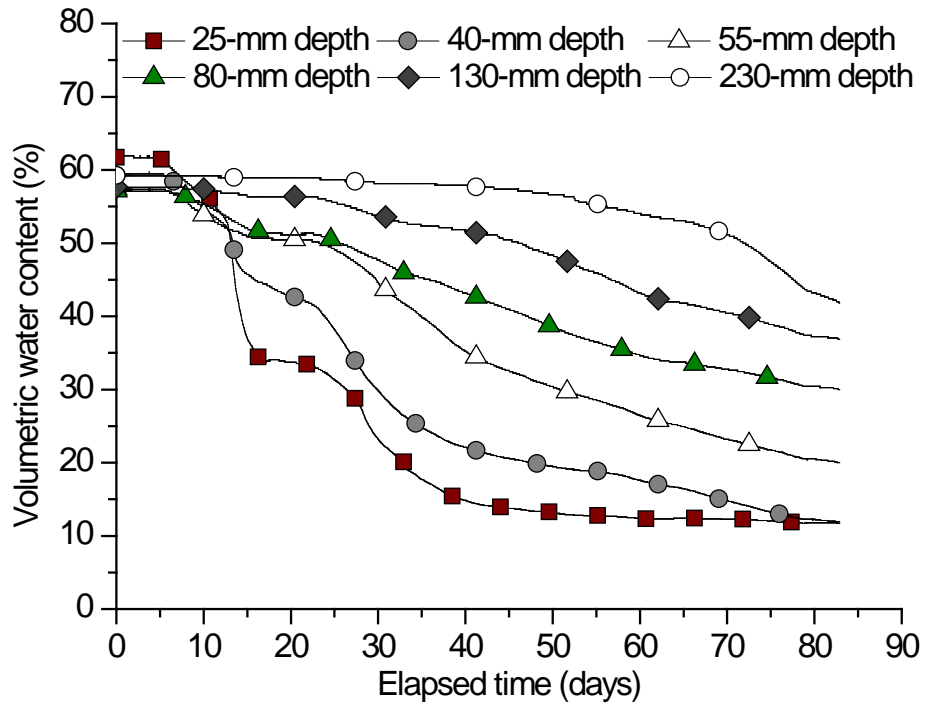
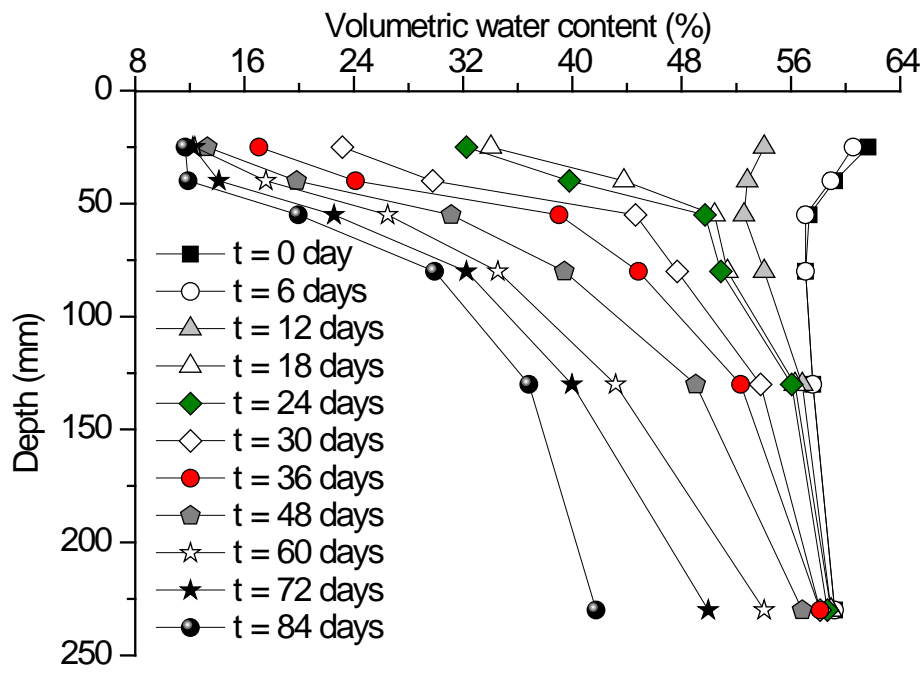
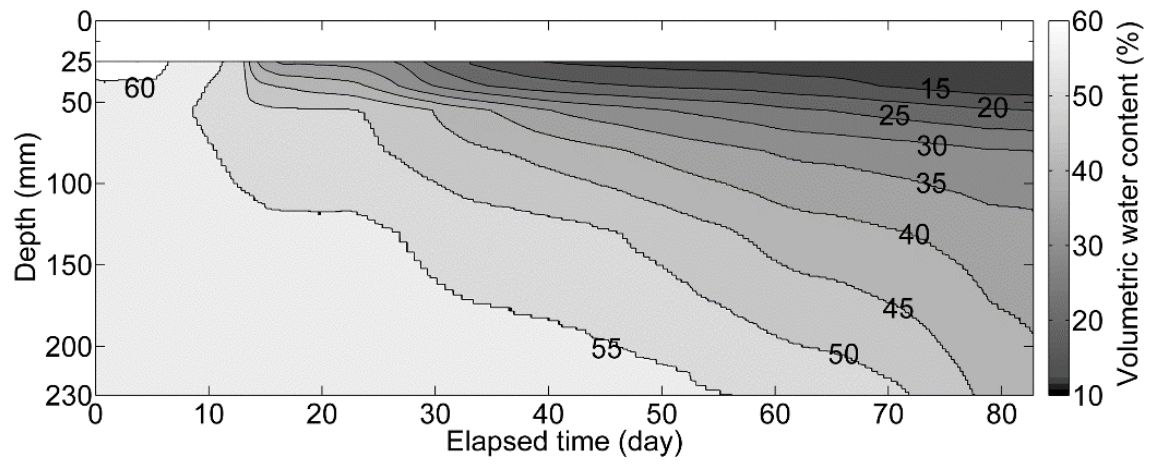


Fig. 14. Evolutions of volumetric water content at different depths



**Fig. 15.** Profiles of volumetric water content



**Fig. 16.** Contour map of volumetric water content at different times

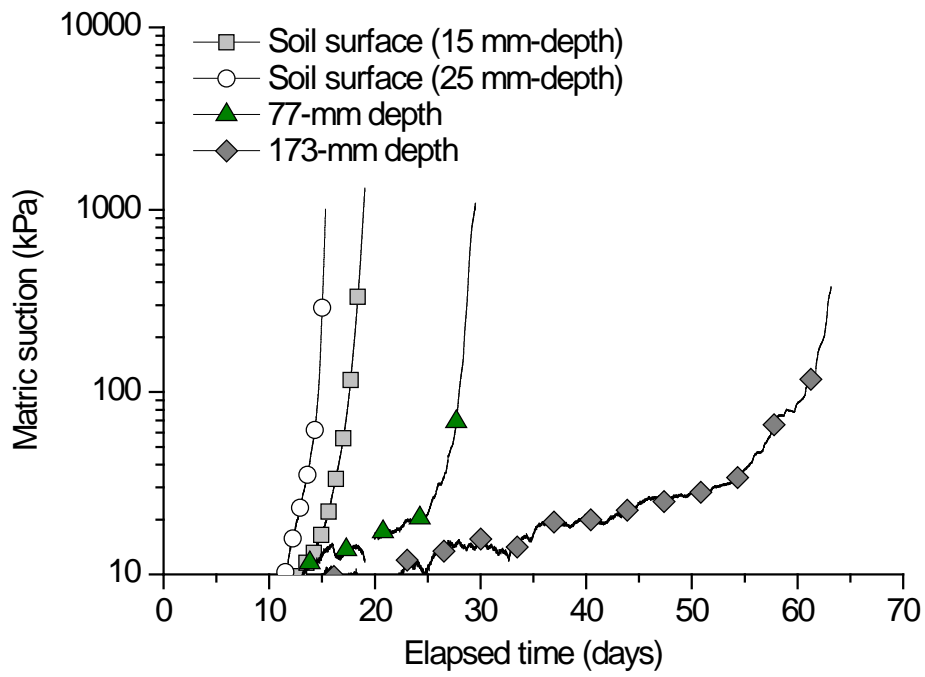


**Fig. 17.** Evolutions of soil matric suction at different depths

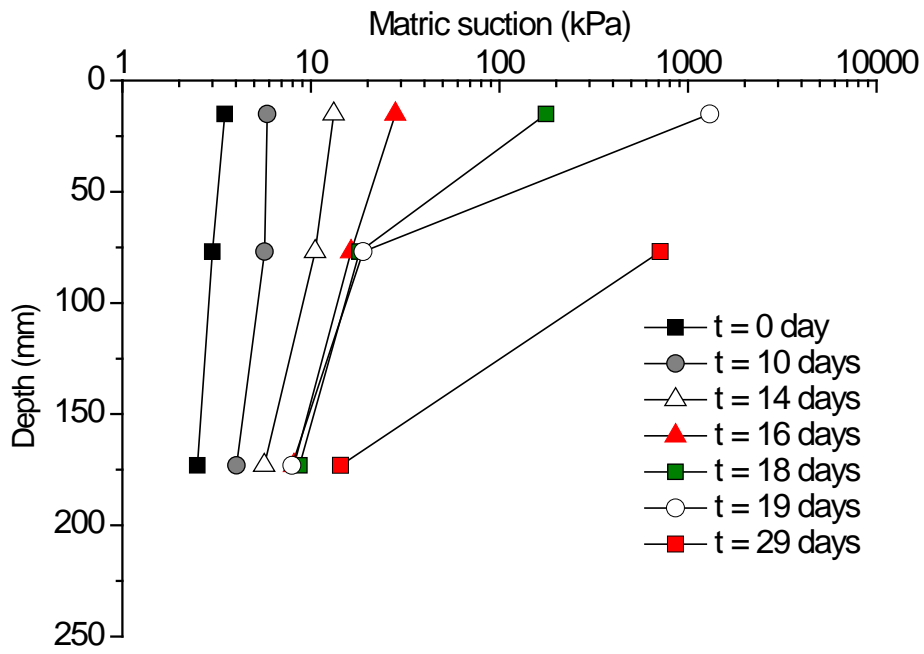
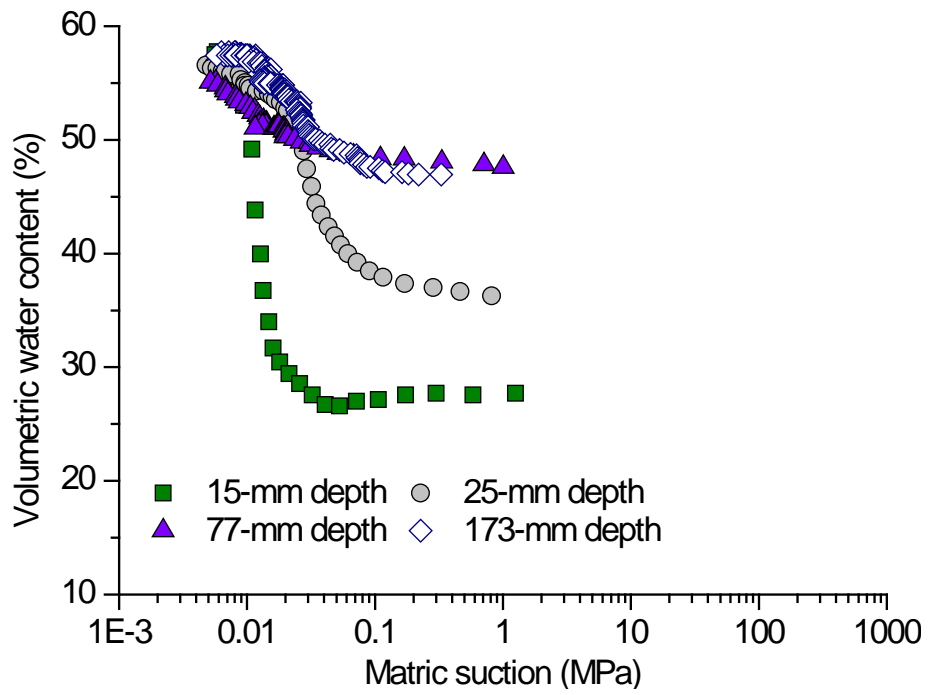
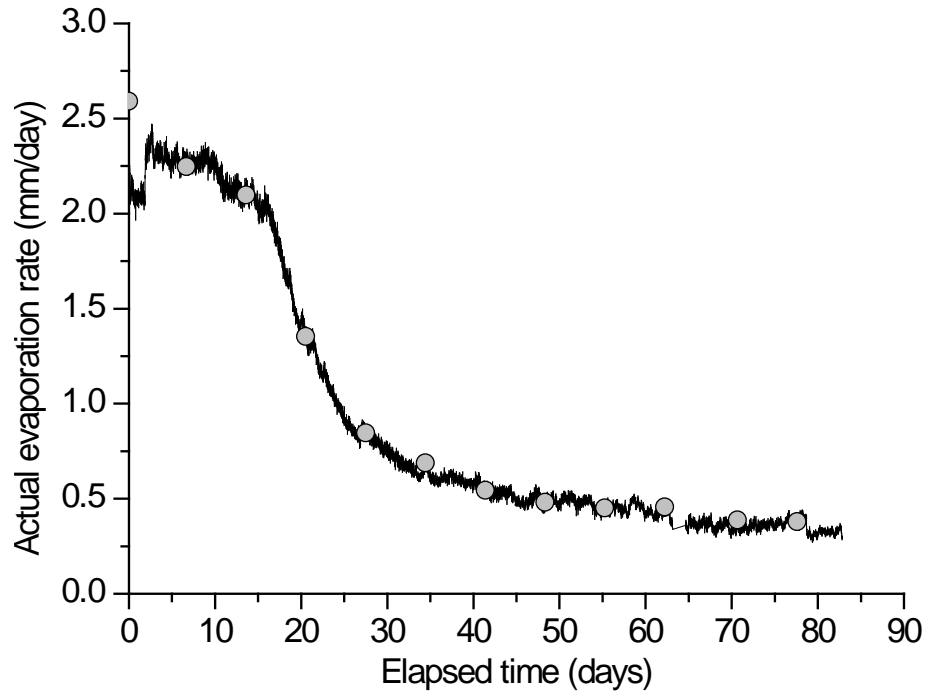


Fig. 18. Profiles of matric suction at different times



**Fig. 19.** Soil water retention curve obtained from the evaporation test



**Fig. 20.** Evolution of actual evaporation rate

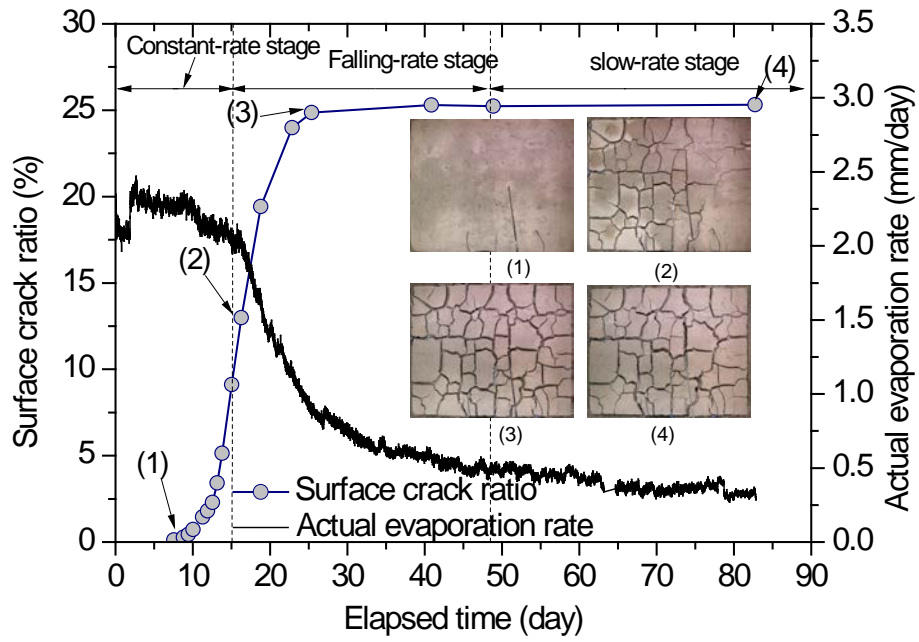


**Fig. 21.** Evolution of surface crack ratio

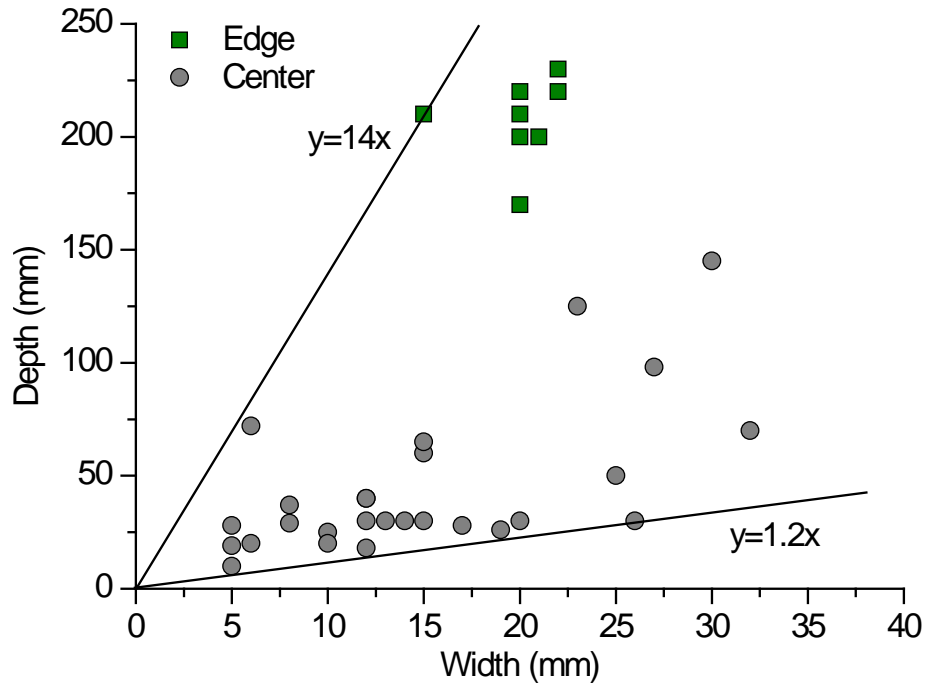


Fig. 22. Depth versus width of crack